HHS Public Access

Author manuscript

Mol Pharm. Author manuscript; available in PMC 2020 April 10.

Published in final edited form as:

Mol Pharm. 2019 February 04; 16(2): 469–479. doi:10.1021/acs.molpharmaceut.7b00484.

Nanoparticle Properties for Delivery to Cartilage: The Implications of Disease State, Synovial Fluid, and Off-Target Uptake

Shannon Brown, **Jake Pistiner**, **Isaac M. Adjei**, **Blanka Sharma***

J. Crayton Pruitt Family Department of Biomedical Engineering, University of Florida, 1275 Center Drive, Biomedical Sciences Building JG-56, P.O. Box 116131, Gainesville, Florida 32611-6131, United States

Abstract

A major hurdle limiting the ability to treat and cure osteoarthritis, a common and debilitating disease, is rapid joint clearance and limited cartilage targeting of intra-articular therapies. Nanoscale drug carriers have the potential to improve therapeutic targeting and retention in the joint after direct injection; however, there still lacks a fundamental understanding of how the physicochemical properties of nanoparticles (NPs) influence localization to the degenerating cartilage and how joint conditions such as disease state and synovial fluid impact NP biodistribution. The goal of this study was to assess how physicochemical properties of NPs influence their interactions with joint tissues and, ultimately, cartilage localization. *Ex vivo* models of joint tissues were used to study how poly(lactide-*co*-glycolide) (PLGA) and polystyrene (PS) NP size, charge, and surface chemistry influence cartilage retention under normal and disease-mimicking conditions. Of the particles investigated, PLGA NPs surface-modified with a quaternary ammonium cation had the greatest retention within cartilage explants; however, retention was diminished 2- to 2.9-fold in arthritic tissue and in the presence of synovial fluid. Interactions with synovial fluid induced changes to NP surface properties and colloidal stability *in vitro*. The impact of NP charge on “off-target” synoviocyte uptake was also dependent on synovial fluid interactions. The results suggest that the design of nanocarriers for targeted drug delivery within the joint cannot be based on a single parameter such as zeta potential or size, and that the fate of injected delivery systems will likely be influenced by the disease state of the joint and the presence of synovial fluid.

Graphical Abstract

*Corresponding Author blanka.sharma@bme.ufl.edu. Phone: (352) 273-9329. Fax: (352) 273-9221.

Supporting Information

The Supporting Information is available free of charge on the ACS Publications website at DOI: 10.1021/acs.molpharmaceut.7b00484.

Penetration depth measurements of NPs into cartilage explants and time progression of synoviocyte uptake of anionic and cationic NPs (PDF)

The authors declare no competing financial interest.

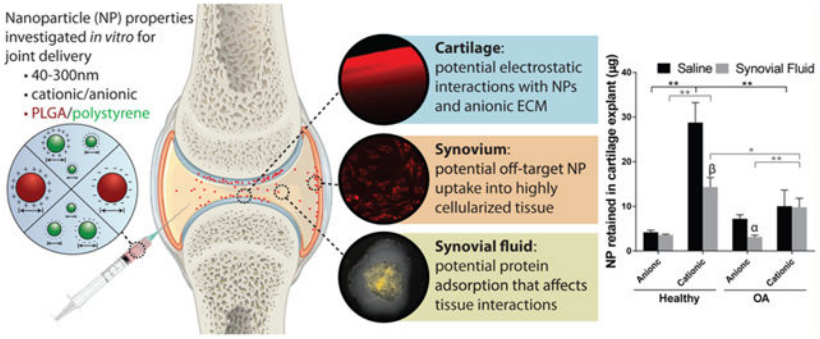

Keywords

Nanoparticle; drug delivery; osteoarthritis; cartilage; synovium; intra-articular; ex vivo models

INTRODUCTION

Drug delivery to osteoarthritic (OA) joints is a pressing and complex challenge facing the medical community. Direct administration of OA therapeutics by intra-articular injection is often elected to overcome the low joint bioavailability of systemically administered drugs.[1] However, many drugs administered via intra-articular injection (i.e., direct injection into the joint) are subject to rapid clearance from the joint space.[2-4] Improvements in joint residence of therapeutics postinjection is crucial as this limitation in availability causes the need for frequent injections, thereby increasing cost, risk of infection, dosing, and clinical demand.[5,6] Common and growing in prevalence, OA currently affects 630 million individuals globally, with United States projections indicating a 30% increase in doctor-diagnosed, self-reported OA within the next 15 years.[7,8] Unfortunately, current therapies are only palliative, and there are no disease-modifying therapies available to patients.

Joints undergoing OA are subject to a complex and perpetuating cycle of inflammation, cartilage extracellular matrix (ECM) degeneration, mechanical stresses, and production of catabolic factors within the intra-articular space..[9,10] A hallmark of OA progression is erosion of the articular cartilage, the products and ECM fragments of which further stimulate inflammation and propagate the disease. Although OA is a disease of the whole joint with multiple potential sites of therapeutic intervention, the cartilage is an important target for attenuating disease progression.[11,12] Agents to slow cartilage degradation[13-19] and regulate chondrocyte metabolism[20-24] have been identified as potential disease-modifying therapeutics, but what is lacking are effective delivery systems to localize these therapeutics to cartilage. Off-target accumulation of injected chondroprotective drugs in the synovium further reduces the drug bioavailability to cartilage and expedites clearance from the joint.[2,25]

Nanoparticle (NP)-based systems offer the potential for enhancing drug localization to cartilage, however, the dense and highly charged ECM poses a barrier for delivery. Recent efforts have produced molecular and protein platforms,[13,26] polymeric NPs,[27-30] and liposomes that have demonstrated varying extents of cartilage localization using passive and

active targeting approaches. Passive targeting utilizes the fundamental nanocarrier physicochemical properties to encourage non-specific facilitation into the destination tissue or cell, and is therefore the foundation for effective nanocarrier design. Active targeting approaches employ specific biochemical moieties to selectively bind to biological components of the target ECM or cell, furthering specificity, efficiency, and longevity of residence at the target. In cancer applications, the optimization of NP size, charge, hydrophobicity, and specific targeting ligands to promote tumor localization is quite advanced.[31,32] Despite the recent surge of interest in improving the retention of therapeutics in joints and, in particular, cartilage for OA treatments, the systematic evaluation of targeting NP approaches lags behind other fields.

Despite some early successes in investigating targeting mechanisms to improve intra-articular drug delivery, there are many questions to be addressed in order to establish the foundational knowledge needed to advance targeted joint therapies. Specifically, the relationship between fundamental nanocarrier properties, joint tissue interactions, and joint biodistribution at different stages of joint disease is not clear. Knowledge of how to tune particle properties to control localization within the joint space is needed to enhance efficacy of drug delivery to cartilage and minimize dosing requirements and off-target effects.[33]

An additional consideration for intra-articular drug delivery is the impact of synovial fluid on drug delivery vehicles, which is often overlooked. Synovial fluid is an ultrafiltrate of plasma primarily composed of hyaluronic acid and serum proteins, as well as phospholipids, growth factors, cytokines, and proteoglycans including lubricin.[34,35] After intra-articular injection, the synovial fluid is the first substance in which therapies come in contact, and its viscosity and complex biological composition could influence NP properties and function in the joint. However, to date, few studies have been conducted to understand how synovial fluid impacts the properties, stability, and targeting/localization of drug carriers.

The objective of this paper is to investigate how nanocarrier size, charge, and surface chemistry affect the interaction with cartilage, synovial fluid, and synoviocytes, to determine which properties are favorable for passive targeting to cartilage. This understanding of particle–tissue interactions will help lay a foundation for advancing targeted drug delivery within the joint. Furthermore, this paper studies the impact of synovial fluid on nanocarrier properties and their ability to interact with joint tissues. Here, two nanoscale delivery platforms were investigated: (1) poly(lactide-*co*-glycolide) (PLGA) NPs, a drug-loadable and clinically relevant polymeric delivery system with tunable properties, and (2) commercially available polystyrene (PS) NPs of varying monodisperse sizes and surface functionalizations, which are useful models for various NP characteristics. We hypothesized that smaller and cationic NPs would have the greatest association with cartilage due to the dense network of ECM components and electrostatic interactions with the anionic glycosaminoglycans in the tissue. Additionally, we hypothesized that the presence of synovial fluid would influence the ability of the NPs to interact with cartilage and synoviocytes.

EXPERIMENTAL SECTION

NP Materials and Formulation.

Dye-loaded PLGA NPs were prepared through a single emulsion and solvent evaporation technique developed previously.[36,37] Briefly, an organic phase was created by dissolving 50:50 ester-terminated PLGA (Durect Corporation, inherent viscosity 0.95–1.2 dL/g) in chloroform with Nile Red dye. An aqueous phase was prepared with poly(vinyl alcohol) (PVA), an anionic polymer, and/or didodecyldimethylammonium bromide (DMAB), a cationic surfactant with a quaternary ammonium and two 12-carbon chains.[38] The PLGA solution was added to an aqueous phase of either 2% PVA (PVA NPs) for negatively charged NPs or 1% PVA + 0.2% DMAB (DMAB NPs) for positively charged NPs. The oil-in-water solution was emulsified by probe sonication (QSonica Q500 model, constant 38% amplitude by automatic adjustment of power with a maximum power of 500 W), and the organic phase was evaporated overnight under constant stirring at 500 rpm. The NPs were recovered via ultracentrifugation at 84,800 rcf in distilled water and lyophilized with 3% sucrose for storage.

To investigate a greater breadth of NP surface functionalizations and monodisperse sizes, PS NPs were purchased from Sigma-Aldrich (50 and 100 nm aminated (NH2) and 30 nm carboxylated (COOH)), ThermoFisher Scientific (30, 40, and 100 nm COOH), and Polysciences (200 nm COOH), containing various fluorescent dyes. Though not suitable for drug delivery, PS NPs provide valuable tools for screening and modeling various NP properties.[39]

NP Characterization.

All NPs were characterized via dynamic light scattering (DLS; Brookhaven Instruments Corporation, NY) and scanning electron microscopy (SEM; Hitachi SU5000). Measurements for DLS were conducted in distilled water at 0.1 mg/mL for size and 0.4 mg/mL for zeta potential at room temperature. Distribution analysis was conducted in IGOR Pro version 6.3.7.2, and log-normal distributions were calculated with an algorithm developed by Bohorquez and Rinaldi.[40] Imaging by SEM was performed using sputter-coated samples that had been lyophilized without sucrose during formulation. Analysis of NP size by SEM imaging was conducted in ImageJ 1.50i.[41] To ensure reliable tracking of NPs in our experiments, release of Nile Red from PLGA NPs was characterized over 48 h. Nile Red-loaded NPs at 1 mg/mL were incubated in saline at 37 °C on an orbital shaker (60 rpm) and protected from light. NP suspensions were centrifuged at 84,800 rcf for 30 min to separate NPs from released cargo, and the supernatants were lyophilized. Nile Red was extracted from the lyophilized samples with methanol for 24 h at room temperature. To quantify initial dye loading, Nile Red was extracted from known masses of lyophilized NPs in methanol for 24 h at room temperature. For both dye release and total dye loading samples, methanol extractions were centrifuged at 3,200 rcf for 10 min. Fluorescence of the supernatants was measured with high performance liquid chromatography (HPLC) as described below for Nile Red detection. Fluorescence was compared to standards processed in the same manner as described above for the samples.

NP Interactions with Synovial Fluid.

The effect of synovial fluid on NP properties was assessed by characterizing the size and zeta potential of the NPs before and after incubation with synovial fluid. For each group, NPs were constituted in saline to 0.625% w/v, and bovine synovial fluid was added to achieve a final concentration of 0.5% w/v, which is a relevant concentration for intra-articular injection in rodents.[30] The suspension was incubated at 37 °C, shaking at 60 rpm for 30 min, and NPs were washed to remove excess synovial fluid components by ultracentrifugation. Characterization via DLS was conducted for untreated and synovial fluid treated NPs as described.

In cases where gross aggregation of NPs occurred in synovial fluid, further visualization and confirmation was conducted by placing NP–synovial fluid suspensions on a glass slide, followed by gentle stirring with a pipet tip. Synovial fluid was lot-matched with that used in surface interaction studies described above. Experiments were further conducted to determine if NP aggregation was due to NP interactions with hyaluronic acid. In these cases, hyaluronic acid (750 kDa to 1.0 MDa, Lifecore Biomedical, Chaska, MN) was dissolved in saline at 1.88 or 3.21 mg/mL, concentrations reported for osteoarthritic and nonarthritic states, respectively.[42] These interactions were observed on the macroscale in triplicate.

Ex Vivo Cartilage Retention Studies.

To determine the relationship between NP properties and retention in cartilage, cartilage biopsy samples were incubated with NPs, and NP retention was quantified. Cartilage was aseptically collected from the femoral condyles and patelloformal grooves of male bovine juveniles (Research 87 Inc., Boylston, MA), and washed in saline with 1% penicillin–streptomycin. As a model of OA, some tissue was enzymatically digested for 30 min in 0.2% collagenase type II, which has been previously shown to mimic the biochemical and mechanical properties of OA cartilage.[43] Tissue was cut into ~2 mm (thickness) × 6 mm (diameter) biopsy samples with the superficial zone intact.

The process for NP–cartilage interaction studies is depicted in Figure 1. Nanoparticles were prepared to 0.5% w/v in saline or synovial fluid, added to the articular surface of the biopsy samples (40 μL), and then incubated for 30 min. After incubation, excess NP suspension was removed and biopsy samples were washed three times with saline. To quantify the mass of particles remaining in the tissue, biopsy samples were chopped, homogenized in water, and lyophilized. Dye was extracted in methanol from the lyophilized samples, and the fluorescence of the extraction was measured by a plate reader (Biotek Synergy HT) or HPLC. Analysis via HPLC was conducted as described below for PS NPs. Fluorescence was compared to that of standards with known NP masses prepared in the same manner as that done for samples. To account for the differences in dye loading efficiency in the different NP formulations, separate standard curves were created from serial dilutions of each type of NP, and NP quantification for each group was conducted based on the respective curve.

To visualize NP penetration into tissue, cross sections of biopsy samples were imaged with fluorescence microscopy. Cross sections were obtained by inverting biopsy samples and cutting approximately 1 mm thick sections from the bottom toward the articular surface to

avoid potentially pushing NPs deeper into the tissue. Sections were kept hydrated with saline during the imaging process. NP penetration was quantified in ImageJ by measuring in triplicate the distance between the articular surface and the point of maximum observed penetration.[41]

Randomly selected biopsy samples were prepared for histological sectioning prior to NP treatment for each animal. Biopsy samples were fixed in 10% neutral buffered formalin, embedded in paraffin, and sectioned for histological analysis. Sections were stained with Safranin-O, counterstained with Fast Green, and sealed in Permount (ThermoFisher Scientific, Hampton, NH).

Evaluation of Chondrocyte Cytotoxicity in Explants.

Cartilage samples for cytotoxicity analysis were collected aseptically as described above, immediately plated in 24-well plates, and placed into incubation at 37 °C and 5% carbon dioxide in chondrocyte medium (high glucose Dulbecco's modified Eagle medium (DMEM) with 10 mM hydroxyethyl piperazineethanesulfonic acid, 0.1 mM nonessential amino acids, 0.4 mM proline, 50 mg/L vitamin C, 10% fetal bovine serum (FBS), and 1% penicillin–streptomycin).

Chondrocyte cytotoxicity was evaluated via 3-(4,5-dimethylthiazol-2-yl)-5-(3-carboxymethoxyphenyl)-2-(4-sulfophenyl)-2*H*-tetrazolium (MTS) CellTiter 96 aqueous proliferation assay (Promega, Madison, WI). Freshly isolated cartilage biopsy samples were cultured for 24 h as described above prior to treatment, and then cultured with varying concentrations of NPs in low serum (1% FBS) DMEM for 24 h. After that time, NP suspensions were removed and replaced with assay reagent prepared according to manufacturer recommendations. After 3 h incubation with the assay reagent, the medium was stirred gently, removed, and plated in triplicate for measurement on a plate reader. Explants were dab-dried and weighed for normalization.

Synoviocyte Isolation, Culture, and NP Uptake.

Synoviocytes were isolated from male juvenile bovine knees (Research 87 Inc., Boylston, MA) according to protocols developed by Haerdi-Landerer et al.[44,45] Sections of synovial membranes were explanted under aseptic conditions, and immediately submerged in sterile saline with 1% penicillin–streptomycin. Explants were washed and cut into ~1–2 mm squares and pretreated in 0.2% trypsin for 30 min followed by an overnight incubation in 0.2% type I collagenase. Incubation was conducted at 37 °C, 5% carbon dioxide, shaking constantly at 40 rpm. Cells were separated from the digested tissue with cell strainers and plated at approximately 1.1×10^4 cells/mm^2 in high glucose DMEM containing 10% FBS and 1% penicillin–streptomycin.

Passage 1 synoviocytes were plated into 24-well plates at 31,500 cells/cm^2 and were cultured for 2 days. Medium was replaced with low-serum medium (1% FBS) containing 20 μg/mL PVA or DMAB NPs and 0%, 10%, or 50% synovial fluid. This NP concentration was selected for its suitable HPLC and microscopy detection without saturating cell uptake at the seeding density utilized. To assess the impact of synovial fluid on NP transport to cells, additional treatments included synovial fluid coated NPs in low-serum medium; PVA and

DMAB NPs had been precoated with synovial fluid in the same manner as for NP–synovial fluid interaction studies. To assess the rate of NP uptake and select time points for uptake quantification, cells were incubated with Nile Red loaded PLGA NPs and imaged via fluorescent microscopy at various times over 12 h. At each time point, wells in triplicate were washed once with DMEM, washed once with saline, and imaged on a fluorescence microscope. Fluorescent microscope settings were uniform across all images. Fluorescence intensity was quantified by measuring the mean gray value in ImageJ Fiji.[46] Based on the kinetics of NP uptake observed in the time course study, NPs were quantified at 2 and 6 h, as these points capture uptake before and after steady state. Cells were washed three times in saline and lysed, after which the lysate was lyophilized, and the dye was extracted from the lysate solids with methanol for 2.5 days. Nile Red fluorescence was quantified via HPLC. Fluorescent NP standards were prepared for each NP type in untreated cell lysate and processed in the same manner as done for the samples. To account for the differences in dye loading, NP uptake was quantified based on independent standard curves generated for each NP formulation. Fluorescence was normalized to DNA content determined via a Quant-iT PicoGreen Assay (ThermoFisher Scientific, Hampton, NH). Controls included synoviocytes cultured with reduced-serum medium without NPs and with 0%, 10%, or 50% synovial fluid and were processed in the same manner as treated samples.

High Performance Liquid Chromatography.

For all analyses, HPLC was conducted in an Acclaim 120 column (C18, 3 μm, 120 Å) with 100% methanol at 1 mL/min. Nile Red associated with PLGA NPs was detected at excitation 552 nm and emission 636 nm during a 6 min run. The commercially prepared PS NPs contained various dyes and were detected with the following excitations/emissions and run times: 50 nm PS NH2 358 nm/410 nm for 13 min; 100 nm PS NH2 481 nm/644 nm for 5.5 min; 40 nm PS COOH 580 nm/605 nm for 8 min; 100 nm PS COOH 505 nm/525 nm for 6 min.

Statistics.

Statistical analysis was conducted in GraphPad PRISM 7.01 (La Jolla, CA). Error bars indicate standard deviations. Unless otherwise stated, statistical comparison of means was conducted in GraphPad via 2-way ANOVAs with Tukey's multiple comparisons tests with outcomes denoted as (*) $p < 0.05$, (**) $p < 0.01$.

RESULTS

NP Properties and Synovial Fluid Interactions.

Nanoparticles were primarily characterized by size and zeta potential, and changes in these properties were assessed after incubation in synovial fluid. Poly(lactide-*co*-glycolide) NPs had an effective hydrodynamic diameter of 260–290 nm (Figure 2A,B), as determined by DLS. Visualization of NPs by SEM illustrated a spherical geometry for all NPs and, as expected, gave diameters smaller than those determined by DLS. By SEM, NPs were 123.3 ± 49.4 nm and 112.4 ± 37.5 nm for anionic PVA and cationic DMAB NPs, respectively. The PVA and DMAB NPs were similar in size, shape, and distribution, but differed in surface charge with zeta potentials of −17.0 and +24.6 mV, respectively (Table 1). The PS NPs were

uniform in size and shape (Figure 2C) with different zeta potentials based on formulation (Table 1). Dye loading in PLGA PVA and DMAB NPs was 24.9 ± 0.04 μg Nile Red/mg NP and 11.54 ± 0.04 μg Nile Red/mg NP, respectively. In subsequent studies, these differences in loading efficiency were accounted for by generating independent standard curves from each NP type. After 48 h of incubation at 37 °C, 3.0% ± 0.4% and 3.5% ± 0.9% of the total dye was released from PVA and DMAB NPs, respectively, indicating that the NPs could be reliably tracked by Nile Red encapsulation for the course of the experiments.

Synovial fluid had a significant impact on NP properties in most cases. Upon incubation with synovial fluid, NPs demonstrated increases in hydrodynamic diameter and changes in zeta (Table 1), with a notable charge reversal in cationic DMAB NPs. Additionally, the standard deviations for these measurements generally increased after incubation with synovial fluid. One exception was anionic PVA NPs, in which both size and charge remained statistically unchanged by DLS characterization. Interestingly, PS NH2 NPs underwent gross irreversible aggregation when in contact with synovial fluid, forming a macroscopic gel (Figure 3). A predominant component of synovial fluid is hyaluronan, which is an anionic, nonsulfated glycosaminoglycan. A follow-up experiment was conducted to determine if PS NH2 aggregation was related to electrostatic interactions with the hyaluronic acid in the synovial fluid. In this experiment, amine functionalized PS NPs were suspended in high molecular weight hyaluronic acid at concentrations comparable to hyaluronic acid in both normal (Figure 3) and arthritic (not shown) joints. Visible aggregation did not occur in these suspensions, suggesting that the association between NPs and synovial fluid is more complex than amine interactions with hyaluronic acid.

Ex Vivo Cartilage Retention Studies.

An *ex vivo* model was developed to evaluate the influence of NP properties on cartilage interactions, and included conditions in which the tissue mimicked the ECM of OA tissue. Histology confirmed surface depletion of proteoglycans in enzymatically treated (“OA”) cartilage compared to untreated (“healthy”) cartilage (Figure 4A). These findings are consistent with models of microscale and biochemical changes in OA cartilage.[43] The PLGA NPs did not induce toxicity in cartilage explants, as determined by MTS assays (Figure 4B). Nanoparticle retention in cartilage was influenced by NP properties, synovial fluid, and tissue conditions. In healthy cartilage, cationic DMAB NPs demonstrated 6-fold greater retention than anionic PVA NPs (Figure 4C). In the presence of synovial fluid, the DMAB NPs demonstrated a 50% reduction in cartilage retention compared with saline; however, they remained 4-fold higher than the corresponding PVA NP retention. Interestingly, cartilage retention of anionic PVA NPs was not affected by synovial fluid. This finding may be related to the observation that PVA NP properties do not change in synovial fluid. The differences between DMAB and PVA NP retention were less pronounced in the OA model of cartilage. In OA cartilage, there was no significant difference between DMAB and PVA NP retention in saline. However, in the presence of synovial fluid, the DMAB NPs demonstrated a 3-fold increase in retention compared to the corresponding PVA NP group.

Cross sections of biopsy samples were imaged to analyze NP penetration and localization within the explant ECM. Fluorescence microscopy of biopsy sample cross sections

corroborated the quantitative retention findings, illustrating greater presence of cationic DMAB NPs relative to anionic PVA NPs, and a reduction in signal with synovial fluid suspended NPs (Figure 4D). Additionally, microscopy illustrated differences in NP penetration into tissue; DMAB and PVA NPs are visible to ~330 μm and ~130 μm below the articular surface of healthy cartilage, respectively (Figure 4D and Figure S1).

Polystyrene NPs were used to further probe size and surface chemistry as modulators of NP–cartilage interactions because of their monodisperse nature and varied surface functionalizations. Tissue health and synovial fluid affected PS NP retention in cartilage (Figure 5); however, the relationship between NP zeta potential and cartilage retention in PS NPs differed from PLGA NPs. For instance, in healthy cartilage, cationic 100 nm NH2 NPs demonstrated 56% greater cartilage retention compared to anionic 100 COOH NPs; however, this trend was reversed at the smaller 40–50 nm PS NP size range. In fact, anionic 40 nm COOH NPs demonstrated greater cartilage retention compared to cationic 50 nm NH2 PS NPs, and comparable cartilage retention to the cationic 100 nm NH2 NPs (Figure 5). No clear trend was observed with respect to PS NP size and cartilage retention. The smaller cationic 50 nm NH2 PS NPs demonstrated reduced cartilage retention compared to cationic 100 nm 50 nm NH2 PS NPs. Conversely, the smaller anionic 40 nm COOH NPs demonstrated enhanced retention relative to the larger anionic 100 nm COOH NPs. Across all PS NP types, retention within cartilage was significantly reduced in OA tissue compared to healthy tissue, and differences across size and surface functionality were no longer observed. The presence of synovial fluid resulted in significant reductions in the retention of COOH PS NPs within healthy cartilage, but not in OA models. The impact of synovial fluid on cartilage retention of NH2 PS NP could not be evaluated due to aggregation in synovial fluid.

Synoviocyte Uptake.

Synoviocytes are actively involved in uptake of foreign particulates in the joint space. Therefore, determining how NP properties impact synoviocyte uptake may be important for understanding the potential for “off-target” uptake. PLGA NPs were evaluated for synoviocyte uptake in saline and synovial fluid conditions. Synoviocyte interactions with PLGA NPs demonstrated differences in NP uptake across culture conditions. The PLGA NPs did not affect cell viability, as determined by the PicoGreen DNA assay (PVA 17.1 ± 4.0 ng/mL DNA; DMAB 17.1 ± 4.2 ng/mL DNA; controls 17.9 ± 4.3 ng/mL DNA; $p > 0.05$ between groups). Fluorescent microscopy showed association of the PLGA NPs with the synoviocytes during culture (Figure 6A). Uptake was most rapid in synovial fluid free conditions, and the rate of uptake slowed after approximately 2 h in all culture conditions (Figure S2). Quantification of cell uptake (Figure 6B) demonstrated increased uptake of cationic DMAB NPs compared with anionic PVA NPs in the absence of synovial fluid. A progressive reduction in NP uptake was observed with increasing synovial fluid concentration, and differences in uptake between DMAB and PVA NPs were not observed in the 10% and 50% synovial fluid groups. Since the presence of synovial fluid may act as a transport barrier in these cultures, uptake studies were also conducted with NPs after coating with synovial fluid proteins to further probe if differences in NP–synovial fluid interactions can impact cell uptake without the influence of viscosity from synovial fluid. Interestingly,

after being coated with synovial fluid, DMAB NPs demonstrated up to a 57% reduction in synoviocyte uptake compared to PVA NPs, and a 55% reduction compared to DMAB NPs in the absence of synovial fluid. Conversely, the PVA NPs experienced up to a 38% increase in synoviocyte uptake after being coated with synovial fluid components compared to PVA NPs in the absence of synovial fluid. Control cultures of synoviocytes with 0%, 10%, and 50% synovial fluid had no detectable fluorescence with microscopy and HPLC.

DISCUSSION

This study highlights several underappreciated challenges for cartilage targeting in NP-based intra-articular drug delivery. Nanoscale drug delivery systems must overcome a complex environment that includes dense and negatively charged cartilage ECM, synovial fluid occupying the joint space, and rapid clearance via the surrounding synovium. In these studies, the impact of NP physicochemical properties on interactions with cartilage and synoviocytes under varying joint conditions was investigated to better understand the NP design criteria and how to strategically guide drugs to cartilage after intra-articular injection. While we hypothesized that smaller and cationic NPs would demonstrate the highest cartilage retention, this was not fully confirmed by the data. In fact, these findings suggest that a multitude of factors must be considered for cartilage targeting.

Honing the fundamental NP design for optimized cartilage drug delivery is critical to progressing the therapeutic arena for OA. The greatest interaction with cartilage was observed with PLGA NPs when exhibiting a cationic surface charge. The increased association may be explained by the electrostatic attraction between cationic NPs and anionic cartilage ECM, which is composed of sulfated proteoglycans. Similar findings have been reported in which cationic agents demonstrate superior association with cartilage *in vitro* without synovial fluid.[48,49] Decoration of NPs with quaternary ammoniums has also been shown to improve NP uptake into the ECM of cartilaginous tumors by passively targeting the rich proteoglycan matrix.[50] However, trends between NP charge and cartilage retention were different in PLGA and PS NPs. These differences in NP systems suggest that other properties such as surface chemistries and/or hydrophilicity play a role to influence the NP interaction with cartilage. For example, NH2 PS and PLGA DMAB surfaces are decorated with primary amines and quaternary ammonium, respectively, and, despite having similar sizes and charges, NH2 PS and PLGA DMAB NPs were retained in the cartilage ECM to different degrees. Surface charge alone is likely not a targeting mechanism universal to all NP systems.

Size is also an important consideration for NP localization in the joint, and there are likely trade-offs between cartilage targeting, penetration, and joint clearance of NPs that impact the efficiency and longevity of NP retention in cartilage. For example, small NPs (<100 nm) may penetrate deeper into cartilage[30,51] but may also be more rapidly cleared from the joint, while larger NPs have less cartilage penetration but may be able to deliver a more sustained payload and accumulate in more permeable tissue regions where degeneration has ensued. In these studies, DMAB NPs (~260 nm by DLS, 112 nm by SEM) had the greatest overall retention, and achieved a penetration depth of ~330 μm from the articular surface. This depth is mostly composed of superficial zone, reported to be the top 7% (or ~130 μm) of

bovine cartilage.[52] While there may be cases in which full penetration into cartilage is desired, superficial zone accumulation *in vivo* still can be advantageous. The superficial zone is the first site of degeneration in OA,[53-55] so immediate delivery to this architectural zone could be opportune. Furthermore, NPs with larger diameters allow for superior drug loading and prolonged release, and cargo intended for cartilage extracellular space can still be transported into the deeper zones as the particles degrade even if the nanocarriers are trapped near the articular surface.

A key consideration of NP design is the state of the joint in which the NPs are to be delivered. Osteoarthritic cartilage is less capable of interacting with or retaining NPs, particularly for cationic NPs. Relative to healthy cartilage, cationic DMAB NPs experienced a 3-fold reduction in retention in OA tissue. These changes in NP retention were likely driven by the structural and biochemical changes of OA cartilage. Histological staining of the enzymatically digested “OA” tissue confirmed a depletion of proteoglycans at the articular surface that would reduce the fixed charge density of the ECM, thereby reducing NP electrostatic association with cartilage. Additionally, digestion of the tissue increases ECM permeability, which may permit NPs to be flushed out during the washing steps, especially without a mechanism of immobilization such as a targeting ligand or electrostatic association. Interestingly, anionic PVA NPs did not demonstrate a reduction in retention in OA cartilage. For PVA NPs, the loss of negatively charged proteoglycans may have reduced electrostatic repulsion and actually facilitated tissue retention, even with an increase in tissue permeability. These changes in NP interactions with OA tissue reinforce the need for investigations with diseased tissue both *ex vivo* and *in vivo*, particularly considering that most *in vivo* studies of nanoscale joint delivery have been conducted in healthy animals.[28,29,56,57]

Our results suggest that synovial fluid is a modulator of NP fate in the joint. It is important to understand how synovial fluid impacts delivery systems for the joint because there are clinical instances in which synovial fluid may or may not be present in the joint space after injection. For example, conventional intra-articular injections of NPs will almost always encounter synovial fluid, even in diseased joints in which synovial fluid is less viscous and less concentrated due to joint catabolism and effusion. However, the design of NPs for application after arthroscopic procedures may not need to account for synovial fluid alterations to particle properties, as the joint is irrigated to remove synovial fluid components.

One mechanism by which synovial fluid impacts NP fate is through changes to the NP surface properties, which suggests macromolecule adsorption onto the particle surfaces. This has implications for intra-articular delivery of nanoscale platforms, as specifically tuned carriers may experience physicochemical alterations after injection into the joint. All NPs were anionic after coating, with cationic DMAB NPs undergoing a complete charge reversal. The observation that anionic PVA NPs did not change while PS NPs of similar size and zeta potential experienced significant increases in diameter and zeta potential suggests that this interaction is likely driven by surface chemistry more so than particle size and charge. Synovial fluid also disrupted the colloidal stability of the cationic NH2 PS NPs, leading to gelation of the particles with synovial fluid components. Despite having similar charge

densities, the PS NPs with primary amines aggregated in synovial fluid; however, the DMAB NPs, comprising quaternary ammonium, did not. This finding suggests differences in the molecular interactions between the NP surface and synovial fluid components that cannot be attributed to charge alone. While some groups have recently taken advantage of nanocarrier destabilization to create hydrogel complexes in the joint,[58,59] these changes to particle properties and stability could negatively influence drug localization by inhibiting penetration of NPs into target tissues or masking targeting moieties.

In addition to nanoscale and macroscale (gelation) changes to NP properties after contact with synovial fluid, synovial fluid influenced NP interactions with cartilage and synoviocytes, likely via multifaceted mechanisms. Synovial fluid is highly viscous and impedes the transport of molecules, which could reduce the ability of NPs in solution to reach their target tissue. Additionally, synovial fluid changes NP properties in manners that discourage retention in cartilage, including increased hydrodynamic diameter, which may reduce diffusion into the dense ECM, and decreased zeta potential, which could reduce electrostatic-based associations with the ECM. This concept is supported by the significant reduction of DMAB NP retention in healthy tissue in the presence of synovial fluid, which may be attributed to the NP charge reversal that diminished electrostatic attraction to the ECM. Synovial fluid did not reduce DMAB NP retention in OA tissue likely because the electrostatic targeting was already diminished by proteoglycan loss in the ECM. Interestingly, there was a significant reduction in PVA NPs in OA tissue despite that synovial fluid coating does not change PVA NP properties, suggesting that decreased mass transport may be the dominant factor in this case.

Even if an ideal NP candidate is identified for sufficient cartilage localization, suppressing off-target delivery in the joint is a critical objective to improve the efficacy of injectable delivery platforms and moderate the drug dosages needed to elicit chondroprotection. The capillaries and lymphatics surrounding the synovium are dominant routes for joint clearance of small and large substances, respectively.[2] In fact, NPs of size and chemical components similar to those studied herein have been shown to accumulate in the synovium, where they interact with synviocytes prior to joint clearance.[60] In this study, synoviocytes served as a model of the synovium to provide insight into the influence of NP properties on off-target accumulation after injection. These studies, again, highlighted the impact of synovial fluid and NP properties. Cationic DMAB NPs exhibited greater synoviocyte uptake than anionic PVA NPs in the absence of synovial fluid, which is consistent with the literature in which cationic NPs usually exhibit greater cell uptake than anionic NPs.[38] Interestingly, there were marked differences in uptake between uncoated (0%) PLGA NPs and PLGA NPs coated with synovial fluid: after coating, PVA NP uptake by synoviocytes was enhanced and DMAB NP uptake was suppressed. Different synovial fluid components may adsorb onto DMAB and PVA NP surfaces, with the corona profile associated with DMAB inhibiting synoviocyte uptake and the PVA profile providing enhanced synoviocyte uptake. Although DLS did not detect significant changes to the PVA NP properties after synovial fluid incubation, synoviocyte uptake findings suggest that the biological components of synovial fluid did impact cellular response to the NPs. This finding is similar to analyses of NPs in other biological media such as serum, where NP zeta potential and the specific makeup of the protein corona significantly correlated to cell association.[61] Further studies are needed to

characterize the corona to fully understand the role of these individual components on tissue targeting.

The influence of synovial fluid on transport may be different *in vivo*, as the joint will be subject to mechanical activity and synovial fluid turnover. Synovial fluid properties also change significantly during disease progression, which was not accounted for in the current study. These studies, however, provide insight into the influence of synovial fluid on particle properties and tissue interactions, and highlight the need for further investigation of these relationships *in vivo* at different stages of disease.

In conclusion, the physicochemical properties of nanoscale delivery platforms affect their interactions with joint tissues, and impact localization to cartilage at different states of degeneration. Cationic surfactants such as DMAB can improve cartilage retention of NPs; however, the efficiency of this cartilage targeting approach is impacted by the presence of synovial fluid and the disease state of the cartilage. Synovial fluid was associated with changes to NP properties and colloidal stability, reductions in NP retention in cartilage, and modulation of NP uptake by synoviocytes. These studies underscore the need for further consideration of synovial fluid as a potential influence on drug delivery vehicle targeting in the joint. Additionally, models of diseased cartilage consistently experienced relatively low NP retention compared to healthy tissue, likely as a result of biochemical and permeability changes to the cartilage ECM. These results may indicate a need to identify more “stable” targets in cartilage that do not change as dramatically over the course of disease or, alternatively, a need to customize drug delivery platforms based on stage of disease. Overall, NPs can be designed to passively target cartilage by tuning physicochemical properties to improve the localization of injectable therapeutics, but numerous other factors such as tissue disease state, synovial fluid, and off-target accumulation should be considered as these conditions modulate the fate of NPs and may modify delivery efficiency and drug efficacy *in vivo*.

Supplementary Material

Refer to Web version on PubMed Central for supplementary material.

ACKNOWLEDGMENTS

This material is based upon work supported by the National Science Foundation Graduate Research Fellowship under Grant No. DGE-1315138. Any opinions, findings, and conclusions or recommendations expressed in this material are those of the authors and do not necessarily reflect the views of the National Science Foundation. Research reported in this publication was also supported by the University of Florida Clinical and Translational Science Institute, which is supported in part by the NIH National Center for Advancing Translational Sciences under Award No. UL1 TR001427. The content is solely the responsibility of the authors and does not necessarily represent the official views of the National Institutes of Health. Additionally, the authors would like to acknowledge Glendon Plumton for the SEM imaging and Shreedevi Kumar for the hyaluronic acid images.

ABBREVIATIONS USED

COOH	carboxylate
DLS	dynamic light scattering

DMAB	didodecyldimethylammonium bromide
DMEM	Dulbecco's modified Eagle medium
ECM	extracellular matrix
FBS	fetal bovine serum
HPLC	high performance liquid chromatography
MTS	3-(4,5-dimethylthiazol-2-yl)-5-(3-carboxymethoxyphenyl)-2-(4-sulfophenyl)-2*H*-tetrazolium
NH2	amine
NP	nanoparticle
OA	osteoarthritis/osteoarthritic
PLGA	poly-(lactide-*co*-glycolide)
PS	polystyrene
PVA	poly(vinyl alcohol)
SEM	scanning electron microscopy

REFERENCES

(1). Bottini M; Bhattacharya K; Fadeel B; Magrini A; Bottini N; Rosato N Nanodrugs to target articular cartilage: an emerging platform for osteoarthritis therapy. Nanomedicine 2016, 12 (2), 255–268. [PubMed: 26707894]

(2). Evans C; Kraus V; Setton L Progress in intra-articular therapy. Nat. Rev. Rheumatol 2014, 10 (1), 11–22. [PubMed: 24189839]

(3). Wallis WJ; Simkin PA; Nelp WB Protein traffic in human synovial effusions. Arthritis Rheum. 1987, 30 (1), 57–63. [PubMed: 3814198]

(4). Simkin PA Synovial perfusion and synovial fluid solutes. Ann. Rheum. Dis 1995, 54, 424–428. [PubMed: 7794054]

(5). Oliver-Welsh L; Griffin JW; Meyer MA; Gitelis ME; Cole BJ Deciding How Best to Treat Cartilage Defects. Orthopedics 2016, 39 (6), 343–350. [PubMed: 27893924]

(6). Ferrari M; Onuoha SC; Pitzalis C Trojan horses and guided missiles: targeted therapies in the war on arthritis. Nat. Rev. Rheumatol 2015, 11, 328–337. [PubMed: 25734971]

(7). Corvelli M; Che B; Saeui C; Singh A; Elisseeff J Biodynamic performance of hyaluronic acid versus synovial fluid of the knee in osteoarthritis. Methods 2015, 84, 90–98. [PubMed: 25858258]

(8). Hootman JM; Helmick CG Projections of US prevalence of arthritis and associated activity limitations. Arthritis Rheum. 2006, 54 (1), 226–229. [PubMed: 16385518]

(9). Bijlsma JWJ; Berenbaum F; Lafeber FPJG Osteoarthritis: An update with relevance for clinical practice. Lancet 2011, 377 (9783), 2115–2126. [PubMed: 21684382]

(10). Allen KD; Adams SB; Setton LA Evaluating intra-articular drug delivery for the treatment of osteoarthritis in a rat model. Tissue Eng., Part B 2010, 16 (1), 81–92.

(11). Philp AM; Davis ET; Jones SW Developing anti-inflammatory therapeutics for patients with osteoarthritis. Rheumatology (Oxford, U. K.) 2016, kew278.

(12). Wang K; Xu J; Hunter DJ; Ding C Investigational drugs for the treatment of osteoarthritis. Expert Opin. Invest. Drugs 2015, 24 (12), 1539–1556.

(13). Hu HY; Lim NH; Ding-Pfennigdorff D; Saas J; Wendt KU; Ritzeler O; Nagase H; Plettenburg O; Schultz C; Nazare M DOTAM Derivatives as Active Cartilage-Targeting Drug Carriers for the Treatment of Osteoarthritis. Bioconjugate Chem. 2015, 26 (3), 383–388.

(14). Larkin J; Lohr TA; Elefante L; Shearin J; Matico R; Su JL; Xue Y; Liu F; Genell C; Miller RE; Tran PB; Malfait AM; Maier CC; Matheny CJ Translational development of an ADAMTS-5 antibody for osteoarthritis disease modification. Osteoarthr. Cartil 2015, 23 (8), 1254–1266. [PubMed: 25800415]

(15). Chiusaroli R; Visentini M; Galimberti C; Casseler C; Mennuni L; Covaceuszach S; Lanza M; Ugolini G; Caselli G; Rovati LC; Visintin M Targeting of ADAMTS5′s ancillary domain with the recombinant mAb CRB0017 ameliorates disease progression in a spontaneous murine model of osteoarthritis. Osteoarthr. Cartil 2013 21 (11), 1807–1810. [PubMed: 23954517]

(16). Chen P; Zhu S; Wang Y; Mu Q; Wu Y; Xia Q; Zhang X; Sun H; Tao J; Hu H; Lu P; Ouyang H The amelioration of cartilage degeneration by ADAMTS-5 inhibitor delivered in a hyaluronic acid hydrogel. Biomaterials 2014, 35 (9), 2827–2836. [PubMed: 24424207]

(17). Chockalingam PS; Sun W; Rivera-Bermudez MA; Zeng W; Dufield DR; Larsson S; Lohmander LS; Flannery CR; Glasson SS; Georgiadis KE; Morris EA Elevated aggrecanase activity in a rat model of joint injury is attenuated by an aggrecanase specific inhibitor. Osteoarthr. Cartil 2011, 19 (3), 315–323. [PubMed: 21163358]

(18). Janusz MJ; Hookfin EB; Brown KK; Hsieh LC; Heitmeyer SA; Taiwo YO; Natchus MG; Pikul S; Almstead NG; De B; Peng SX; Baker TR; Patel V Comparison of the pharmacology of hydroxamate- and carboxylate-based matrix metalloproteinase inhibitors (MMPIs) for the treatment of osteoarthritis. Inflammation Res. 2006, 55 (2), 60–65.

(19). Settle S; Vickery L; Nemirovskiy O; Vidmar T; Bendele A; Messing D; Ruminski P; Schnute M; Sunyer T Cartilage degradation biomarkers predict efficacy of a novel, highly selective matrix metalloproteinase 13 inhibitor in a dog model of osteoarthritis: Confirmation by multivariate analysis that modulation of type ii collagen and aggrecan degradation pepti. Arthritis Rheum. 2010, 62 (10), 3006–3015. [PubMed: 20533541]

(20). Mobasheri A The future of osteoarthritis therapeutics: Emerging biological therapy. Curr. Rheumatol. Rep 2013, 15 (12), 385. [PubMed: 24170255]

(21). Li Y; Wang Y; Chubinskaya S; Schoeberl B; Florine E; Kopesky P; Grodzinsky AJ Effects of insulin-like growth factor-1 and dexamethasone on cytokine-challenged cartilage: Relevance to post-traumatic osteoarthritis. Osteoarthr. Cartil 2015, 23 (2), 266–274. [PubMed: 25450855]

(22). Lohmander LS; Hellot S; Dreher D; Krantz EFW; Kruger DS; Guermazi A; Eckstein F Intraarticular sprifermin (recombinant human fibroblast growth factor 18) in knee osteoarthritis: a randomized, double-blind, placebo-controlled trial. Arthritis Rheumatol. 2014, 66 (7), 1820–1831. [PubMed: 24740822]

(23). Chia S-L; Sawaji Y; Burleigh A; McLean C; Inglis J; Saklatvala J; Vincent T Fibroblast growth factor 2 is an intrinsic chondroprotective agent that suppresses ADAMTS-5 and delays cartilage degradation in murine osteoarthritis. Arthritis Rheum. 2009, 60 (7), 2019–2027. [PubMed: 19565481]

(24). Hunter DJ; Pike MC; Jonas BL; Kissin E; Krop J; McAlindon T Phase 1 safety and tolerability study of BMP-7 in symptomatic knee osteoarthritis. BMC Musculoskeletal Disord. 2010, 11 (1), 232.

(25). Janssen M; Mihov G; Welting T; Thies J; Emans P Drugs and Polymers for Delivery Systems in OA Joints. Polymers 2014, 6, 799–819.

(26). Bajpayee AG; Quadir MA; Hammond PT; Grodzinsky AJ Charge based intra-cartilage delivery of single dose dexamethasone using Avidin nano-carriers suppresses cytokine-induced catabolism long term. Osteoarthr. Cartil 2016, 24 (1), 71–81. [PubMed: 26211608]

(27). Sacchetti C; Liu-Bryan R; Magrini A; Rosato N; Bottini N; Bottini M Polyethylene-Glycol-Modified Single-Walled Carbon Nanotubes for Intra-Articular Delivery to Chondrocytes. ACS Nano 2014 8 (12), 12280–12291. [PubMed: 25415768]

(28). Whitmire RE; Scott Wilson D; Singh A; Levenston ME; Murthy N; García AJ Self-assembling nanoparticles for intra-articular delivery of anti-inflammatory proteins. Biomaterials 2012, 33 (30), 7665–7675. [PubMed: 22818981]

(29). Singh A; Agarwal R; Diaz-Ruiz CA; Willett NJ; Wang P; Lee LA; Wang Q; Guldberg RE; Garcia AJ Nanoengineered particles for enhanced intra-articular retention and delivery of proteins. Adv. Healthcare Mater 2014, 3 (10), 1562–1567.

(30). Rothenfluh D; Bermudez H; O'Neil CP; Hubbell J Biofunctional polymer nanoparticles for intra-articular targeting and retention in cartilage. Nat. Mater 2008, 7 (3), 248–254. [PubMed: 18246072]

(31). Maiolo D; Bergese P; Mahon E; Dawson KA; Monopoli MP Surfactant Titration of Nanoparticle–Protein Corona. Anal. Chem 2014, 86 (24), 12055–12063. [PubMed: 25350777]

(32). Sahneh FD; Scoglio CM; Monteiro-Riviere NA; Riviere JE Predicting the impact of biocorona formation kinetics on interspecies extrapolations of nanoparticle biodistribution modeling. Nanomedicine 2015, 10 (1), 25–33. [PubMed: 25032980]

(33). Eichaker LR; Cho H; Duvall CL; Werfel TA; Hasty KA Future nanomedicine for the diagnosis and treatment of osteoarthritis. Nanomedicine (London, U. K.) 2014, 9 (14), 2203–2215.

(34). Daniel M Boundary cartilage lubrication: review of current concepts. Wien. Med. Wochenschr 2014, 164 (5–6), 88–94. [PubMed: 24081750]

(35). Hui AY; McCarty WJ; Masuda K; Firestein GS; Sah RLA systems biology approach to synovial joint lubrication in health, injury, and disease. Wiley Interdiscip. Rev. Syst. Biol. Med 2012, 4 (1), 15–37. [PubMed: 21826801]

(36). Sharma B; Peetla C; Adjei IM; Labhasetwar V Selective biophysical interactions of surface modified nanoparticles with cancer cell lipids improve tumor targeting and gene therapy. Cancer Lett. 2013, 334 (2), 228–236. [PubMed: 23523612]

(37). Sharma B; Ma W; Adjei IM; Panyam J; Dimitrijevic S; Labhasetwar V Nanoparticle-mediated p53 gene therapy for tumor inhibition. Drug Delivery Transl. Res 2011, 1 (1), 43–52.

(38). Peetla C; Labhasetwar V Effect of molecular structure of cationic surfactants on biophysical interactions of surfactant-modified nanoparticles with a model membrane and cellular uptake. Langmuir 2009, 25 (4), 2369–2377. [PubMed: 19161268]

(39). Grafmueller S; Manser P; Diener L; Maurizi L; Diener P-A; Hofmann H; Jochum W; Krug HF; Buerki-Thurnherr T; von Mandach U; Wick P Transfer studies of polystyrene nanoparticles in the ex vivo human placenta perfusion model: key sources of artifacts. Sci. Technol. Adv. Mater 2015, 16 (4), 044602. [PubMed: 27877820]

(40). Bohorquez AC; Rinaldi C In Situ Evaluation of Nanoparticle–Protein Interactions by Dynamic Magnetic Susceptibility Measurements. Part. Part. Syst. Charact 2014, 31, 561–570.

(41). Schneider CA; Rasband WS; Eliceiri KW NIH Image to ImageJ: 25 years of image analysis. Nat. Methods 2012, 9 (7), 671–675. [PubMed: 22930834]

(42). Decker R; Koyama E; Enomoto-Iwamoto M; Maye P; Rowe D; Zhu S; Schultz P; Pacifici M Mouse limb skeletal growth and synovial joint development are coordinately enhanced by Kartogenin. Dev. Biol 2014, 395 (2), 255–267. [PubMed: 25238962]

(43). Griffin DJ; Vicari J; Buckley MR; Silverberg JL; Cohen I; Bonassar LJ Effects of enzymatic treatments on the depth-dependent viscoelastic shear properties of articular cartilage. J. Orthop. Res 2014, 32 (12), 1652–1657. [PubMed: 25196502]

(44). Haerdi-Landerer MC; Suter MM; Steiner A; Wittenbrink MM; Pickl A; Gander BA In vitro cell compatibility and antibacterial activity of microencapsulated doxycycline designed for improved localized therapy of septic arthritis. J. Antimicrob. Chemother 2008, 61 (2), 332–340. [PubMed: 18174200]

(45). Haerdi-Landerer MC; Steiner A; Suter MM Primary bovine synoviocyte cultures: A useful tool for in vitro drug testing? Vet. J2011, 188 (1), 58–63. [PubMed: 20347355]

(46). Schindelin J; Arganda-Carreras I; Frise E; Kaynig V; Longair M; Pietzsch T; Preibisch S; Rueden C; Saalfeld S; Schmid B; Tinevez J-Y; White DJ; Hartenstein V; Eliceiri K; Tomancak P; Cardona A Fiji: an open-source platform for biological-image analysis. Nat. Methods 2012, 9 (7), 676–682. [PubMed: 22743772]

(47). Decker B; McGuckin WF; McKenzie BF; Slocumb CH Concentration of hyaluronic acid in synovial fluid. Clin. Chem 1959, 5, 465–469. [PubMed: 13815294]

(48). Bajpayee AG; Wong CR; Bawendi MG; Frank EH; Grodzinsky AJ Avidin as a model for charge driven transport into cartilage and drug delivery for treating early stage post-traumatic osteoarthritis. Biomaterials 2014, 35 (1), 538–549. [PubMed: 24120044]

(49). Sterner B; Harms M; Wöll S; Weigandt M; Windbergs M; Lehr CM The effect of polymer size and charge of molecules on permeation through synovial membrane and accumulation in hyaline articular cartilage. Eur. J. Pharm. Biopharm 2016, 101, 126–136. [PubMed: 26876928]

(50). Miot-Noirault E; Vidal A; Morlieras J; Bonazza P; Auzeloux P; Besse S; Dauplat MM; Peyrode C; Degoul F; Billotey C; Lux F; Rédini F; Tillement O; Chezal JM; Kryza D; Janier M Small rigid platforms functionalization with quaternary ammonium: Targeting extracellular matrix of chondrosarcoma. Nanomedicine 2014, 10 (8), 1887–1895. [PubMed: 24972007]

(51). Elsaid KA; Ferreira L; Truong T; Liang A; Machan J; D'Souza GG Pharmaceutical nanocarrier association with chondrocytes and cartilage explants: Influence of surface modification and extracellular matrix depletion. Osteoarthr. Cartil 2013, 21 (2), 377–384. [PubMed: 23186944]

(52). Pedersen DR; Goetz JE; Kurriger GL; Martin JA Comparative digital cartilage histology for human and common osteoarthritis models. Orthop. Res. Rev 2013, 5, 13–20.

(53). Buckwalter JA; Mankin HJ; Grodzinsky AJ Articular cartilage and osteoarthritis. AAOS Instruct. Course Lect 2005, 465–480.

(54). French MM; Athanasiou KA Differentiation Factors and Articular Cartilage Regeneration. Top. Tissue Eng 2003, 1–19.

(55). Goldring MB Update on the biology of the chondrocyte and new approaches to treating cartilage diseases. Best Pract. Res. Clin. Rheumatol 2006, 20 (5), 1003–1025. [PubMed: 16980220]

(56). Bajpayee AG; Scheu M; Grodzinsky AJ; Porter RM Electrostatic interactions enable rapid penetration, enhanced uptake and retention of intra-articular injected avidin in rat knee joints. J. Orthop. Res 2014, 32 (8), 1044–1051. [PubMed: 24753019]

(57). Bajpayee AG; Scheu M; Grodzinsky AJ; Porter RM A rabbit model demonstrates the influence of cartilage thickness on intra-articular drug delivery and retention within cartilage. J. Orthop. Res 2015, 33 (5), 660–667. [PubMed: 25627105]

(58). Morgen M; Tung D; Boras B; Miller W; Malfait AM; Tortorella M Nanoparticles for improved local retention after intra-articular injection into the knee joint. Pharm. Res 2013, 30 (1), 257–268. [PubMed: 22996566]

(59). Kim SR; Ho MJ; Lee E; Lee JW; Choi YW; Kang MJ Cationic PLGA/Eudragit RL nanoparticles for increasing retention time in synovial cavity after intra-articular injection in knee joint. Int. J. Nanomed 2015, 10, 5263–5271.

(60). Horisawa E; Kubota K; Tuboi I; Sato K; Yamamoto H; Takeuchi H; Kawashima Y Size-Dependency of DL-Lactide Glycolide Copolymer Particulates for intra-Articular Delivery System on Phagocytosis in Rat Synovium. Pharm. Res 2002, 19 (2), 132–139. [PubMed: 11883639]

(61). Liu R; Jiang W; Walkey CD; Chan WCW; Cohen Y Prediction of nanoparticles-cell association based on corona proteins and physicochemical properties. Nanoscale 2015, 7, 9664–9675. [PubMed: 25959034]

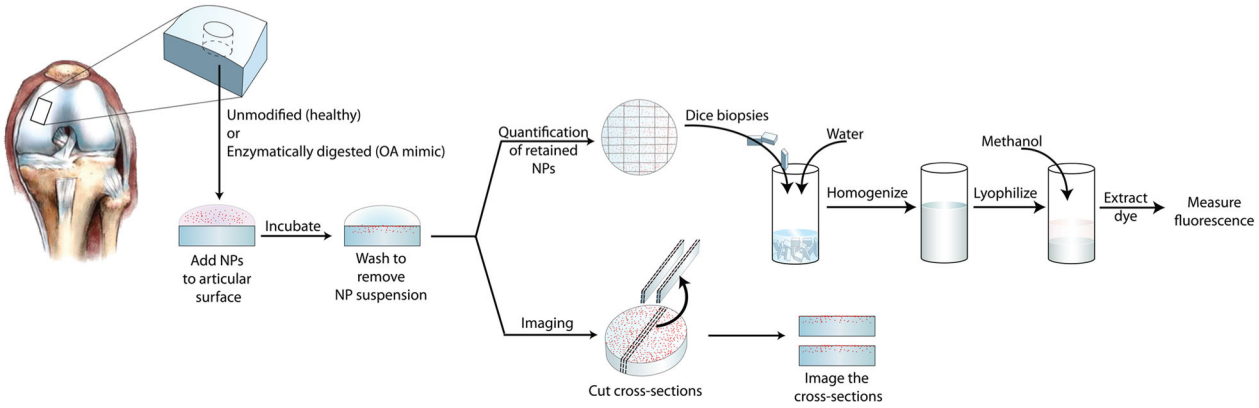

Figure 1.

Schematic of screening technique to evaluate the degree to which NPs interact with cartilage.

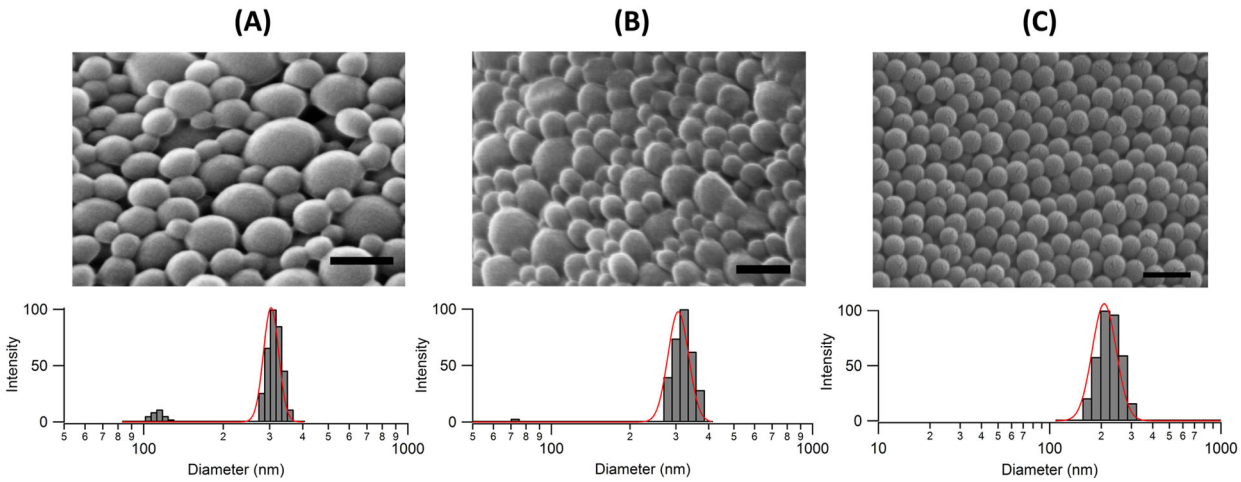

Figure 2.

Physical properties of the different NP types: (A) PVA, (B) DMAB, and (C) 100 nm PS NPs as a representative of the PS NPs. Top: SEM images, scale bar = 200 nm. Bottom: intensity-weighted DLS histograms of hydrodynamic diameters with a log-normal distribution (red).

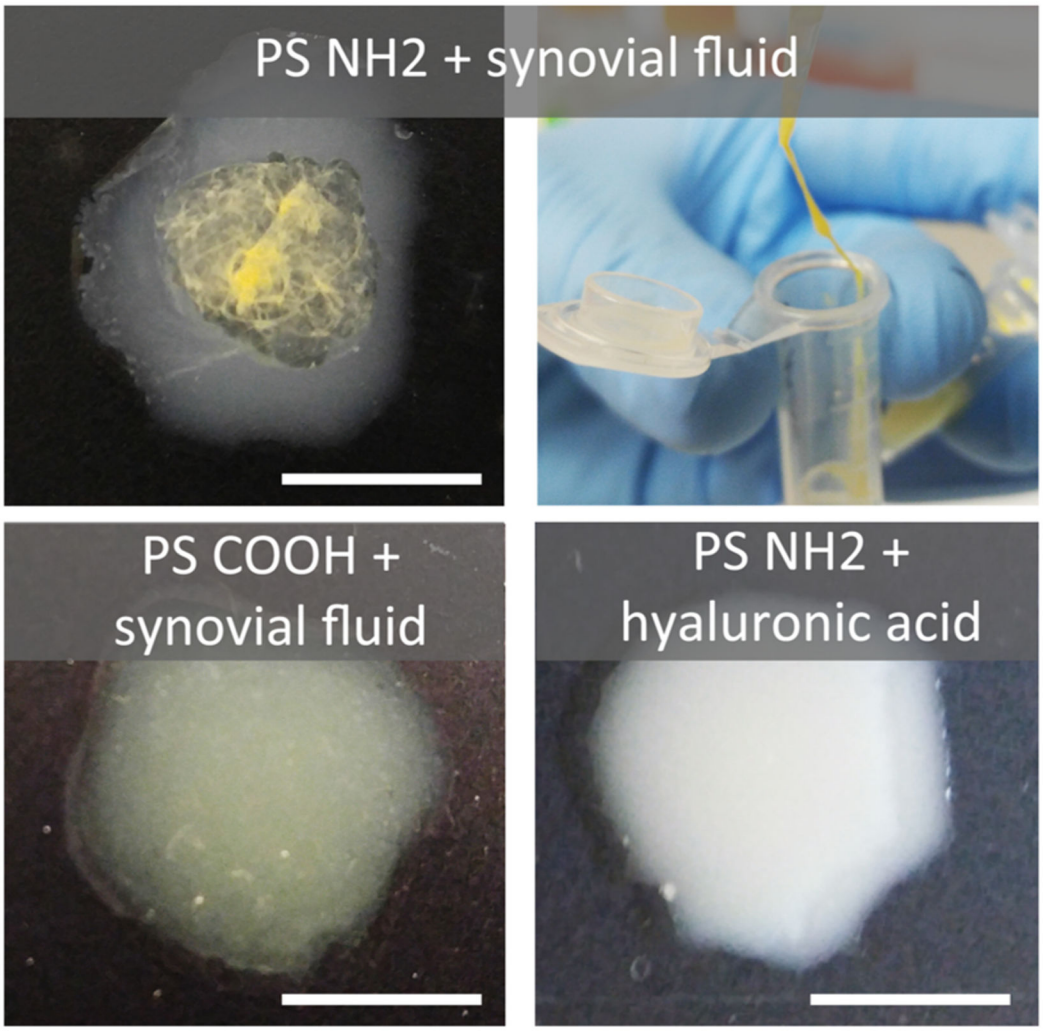

Figure 3.

Aggregation of PS NPs in synovial fluid. Aminated PS NPs showed immediate destabilization and agglomeration in synovial fluid (top), while COOH NPs remained stable (bottom left). When suspended in a solution of 3.21 mg/mL hyaluronic acid in saline, the reported concentration for healthy joints,[47] the aminated particles did not undergo destabilization (bottom right). Gross appearance of PS NH2 was the same when suspended in healthy and osteoarthritic (1.88 mg/mL, not shown) concentrations of hyaluronic acid. Scale bar = 1 cm.

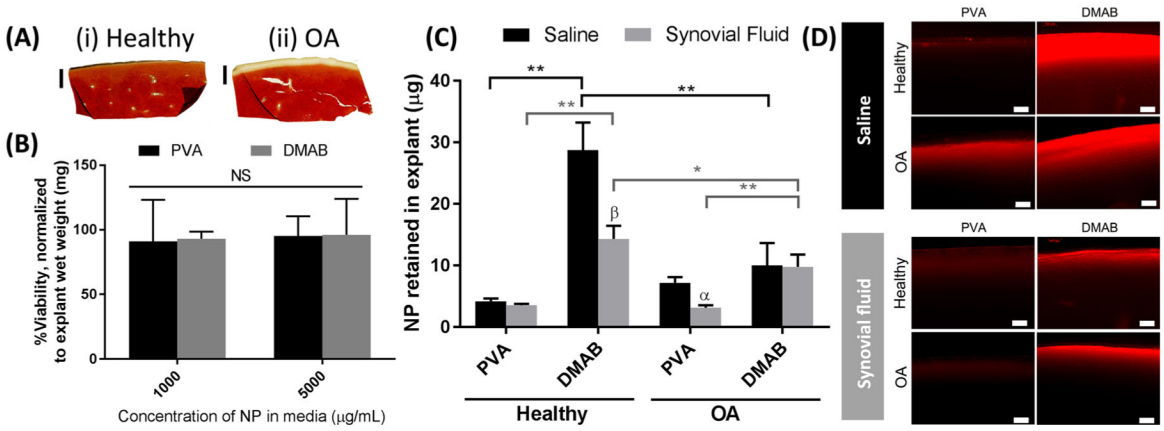

Figure 4.

Ex vivo cartilage retention studies for PLGA NPs, showing the degree of interaction between NPs and cartilage. (A) Histological sections of biopsy samples for (i) fresh cartilage and (ii) enzymatically digested "OA" tissue, stained with Safranin-O and Fast Green. (B) Cytotoxicity of PLGA NPs cartilage corrected for background absorption, reported as a percentage of cellular activity in NP-free conditions, and normalized to explant wet weight ($n = 6$). (C) Quantification of NPs after incubation on cartilage and washing ($n = 5$). (D) Cross sections of fresh biopsy samples imaged with a fluorescence microscope, 20× magnification. Biopsy samples are oriented with the articular surface facing up. Scale bars = 100 μm. (α) $p < 0.05$, (β) $p < 0.01$ between saline and synovial fluid treatments for a single NP group via a 2-way ANOVA with a Holm–Sidak multiple comparisons test. NS = no statistical difference by a 2-way ANOVA.

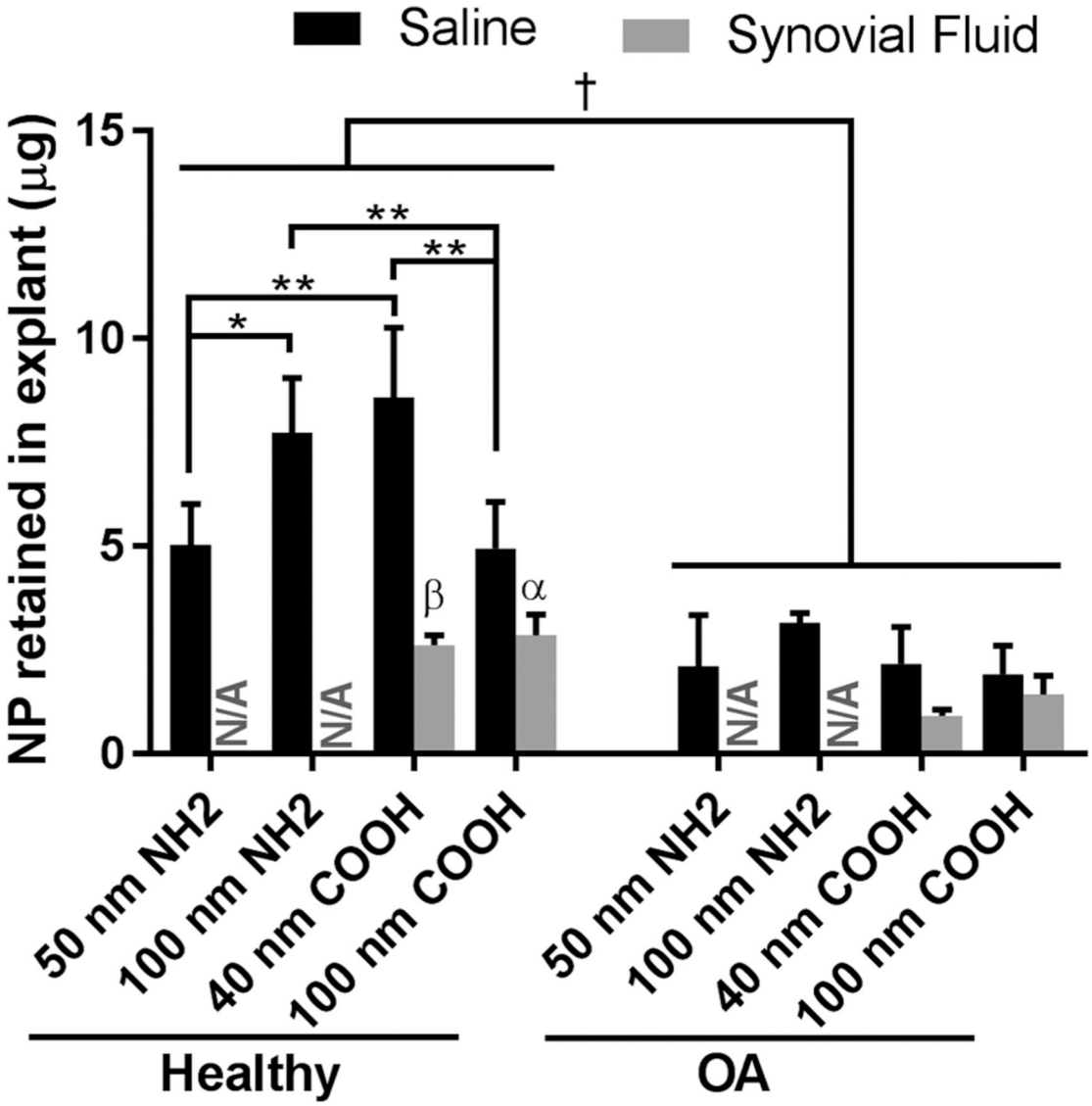

Figure 5.

Quantification of *ex vivo* cartilage retention for PS NPs ($n = 5$). (†) $p < 0.01$ between healthy and OA conditions for all saline-suspended PS NPs via a 2-way ANOVA. (*) $p < 0.05$, (**) $p < 0.01$ via a 2-way ANOVA with a Tukey's multiple comparisons test. (α) $p < 0.05$, (β) $p < 0.01$ between saline and synovial fluid treatments for a single NP group via 2-way ANOVA with a Tukey's multiple comparisons test. N/A = did not conduct analysis of PS NH2 in synovial fluid because of particle destabilization.

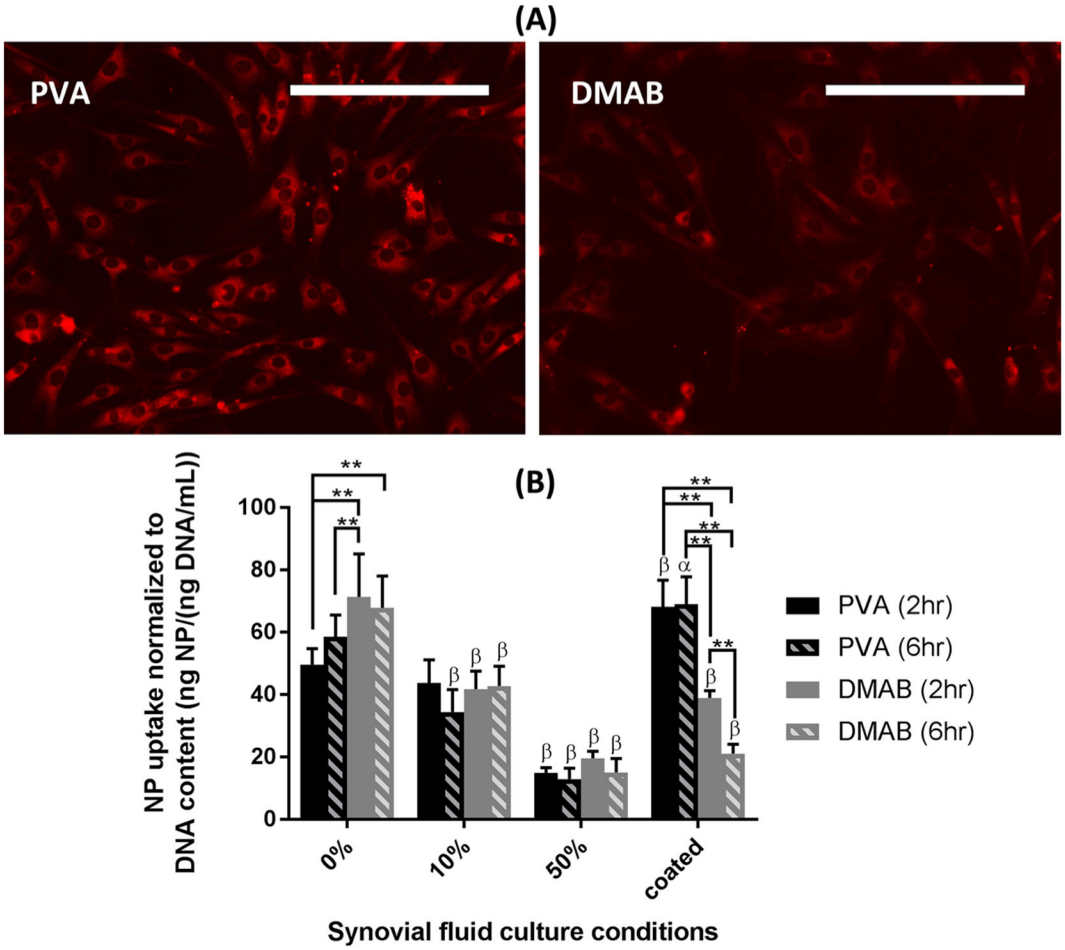

Figure 6.

Synoviocyte uptake of NPs (A) imaged after a single wash with fluorescence microscopy (0% synovial fluid, 6 h incubation) and (B) quantified by HPLC on extracts from cell lysis after four washes ($n = 6$). Fluorescence normalized to DNA content determined via PicoGreen assay. (α) $p < 0.05$, (β) $p < 0.01$ for an individual treatment condition relative to 0% synovial fluid via Dunnett's tests. Scale bar = 200 μm. Note that the fluorescence intensity between micrographs of PVA and DMAB NPs cannot be directly compared due to differences in dye loading efficiencies of the two formulations. NP quantification, however, was done using independent standard curves to account for these differences.

Table 1.

Change in Size and Charge of Various NPs after Incubation with Synovial Fluid ($n = 3$)[a]

	hydrodynamic diameter (nm)			zeta potential (mV)		
NP type and reported size (for PS NPs)	**before**	**after**	**% change**	**before**	**after**	**% change**
PLGA PVA	297.1 ± 4.1	292.1 ± 2.9	−2	−17.0 ± 1.8	−16.5 ± 1.2	−3
PLGA DMAB	261.5 ± 1.7	300.6 ± 1.8	15**	+24.6 ± 0.9	−10.9 ± 1.9	−144**
PS 30 nm COOH	58.9 ± 4.7	104.7 ± 33.8	78	−45.4 ± 2.3	−33.6 ± 5.4	26*
PS 40 nm COOH	61.6 ± 0.8	110.7 ± 1.3	80**	−23.2 ± 5.6	−26.9 ± 2.1	−16
PS 100 nm COOH	202.2 ± 3.2	294.3 ± 4.6	46**	−34.1 ± 5.1	−30.1 ± 0.8	12
PS 200 nm COOH	171.1 ± 1.1	255.0 ± 3.1	49**	−16.7 ± 1.1	−34.9 ± 2.1	−109**
PS 50 nm NH2	57.4 ± 2.3	N/A	N/A	+25.1 ± 1.5	N/A	N/A
PS 100 nm NH2	123.6 ± 1.0	N/A	N/A	+44.3 ± 2.3	N/A	N/A

[a]The hydrodynamic diameter is the effective diameter calculated via the DLS software. Reported size for PS NPs provided by vendor as an approximation determined by SEM. N/A = unable to measure because of aggregation.

(*) $p < 0.05$

(**) $p < 0.01$ by Student's *t*-tests.